Enhanced performance of 40Gbit/s-80GHz OFDM based radio over FSO transmission link incorporating mode division multiplexing under strong atmospheric turbulence

MEHTAB SINGH*, JYOTEESH MALHOTRA
Electronics and Communication Engineering Department, Guru Nanak Dev University, Regional Campus, Jalandhar, India

In this work, we report modeling and performance investigation of 40Gbit/s-80GHz orthogonal frequency division multiplexing (OFDM) based radio over free space optics (RoFSO) transmission system by incorporating mode division multiplexing (MDM) of two Hermite Gaussian (HG) modes (HG01 and HG03) under strong atmospheric turbulence conditions. Two independent 40GHz radio signals each optically modulated at 20Gbit/s are transmitted over free space channel under the impact of dynamic weather conditions and increasing beam divergence angle. Further, the decomposition of distinct HG channels at the receiver unit has been demonstrated. Also, an enhanced performance by using a Square root module (SRm) after the photodiode at the receiving unit has been proposed. The simulation results exhibit a significant improvement in the performance of the link in terms of SNR and total received power by using the proposed system.

(Received November 8, 2018; accepted August 20, 2019)

Keywords: Orthogonal frequency division multiplexing, Mode division multiplexing, Hermite Gaussian modes, Radio over free space optics, Atmospheric turbulence, Square root module

1. Introduction

The last few years have seen an enormous growth in the broadband networks around the world. The trend towards higher data transmission rates in the evolution of 5G networks has led to rapid innovations in optical transmission systems to support a high number of users. The rise in the internet traffic density along with the growth in the number of subscribers and a variety of large bandwidth consuming applications such as video conferencing, high-speed internet etc. have put pressure on low-speed optical transmission links. This calls for a revolution in the traditional optical fiber links in order to support high data rates and increased link coverage. The exponential increase in the number of subscribers each year is posing a great difficulty for the International Telecommunication Union (ITU) to allocate limited radio frequency (RF) spectrum efficiently and reliably among the users. According to ITU, the total number of internet subscribers around the globe in the year 2016 is reported to be 3385 million [1]. Radio over free space optics (RoFSO) can be considered as a promising solution to enhance the broadband capacity, enabling the transmission of a number of RF signals by optically modulating them with high-speed carriers without the need of RF licensing and laying of optical cables. RoFSO exploits the merits of both radio-over-fiber (RoF) technology and free space optics (FSO) links. The merits of RoFSO links include high-speed links, immunity to electromagnetic interference, no need of laying highly expensive optical fiber cables, no need of spectrum licensing, quick and low cost of deployment, secure links, and high channel capacity and bandwidth [2-7]. Thus the incorporation of RoF technology with FSO links can provide a pervasive platform for the integration of wireless networks with optical links to enhance the data transmission capacity of wireless network mobile subscribers quickly and cost-effectively [8]. On the other hand, orthogonal frequency division multiplexing (OFDM) is another information transmission technology in which the information is transmitted over multiple sub-carriers each separated at precise frequencies from each other and having overlapping bands. The sub-carriers used in OFDM technology are orthogonal to each other which prevent the receiver terminals to intercept frequencies other than their own frequency. The orthogonality is achieved using Fast Fourier Transformation (FFT) algorithm. The orthogonality of the sub-carriers results in high-speed long-reach links without any inter-carrier interference [9-14].

In order to enhance the data carrying capacity of the link, mode division multiplexing (MDM) has been exploited as a secure and cost-effective technique by many researchers. In MDM, multiple information channels are transported simultaneously over distinct spatial laser modes excited by optical signal processing techniques [15-

17], spatial light modulators (SLMs) [18, 19], single mode fiber (SMF) [20], and photonic crystal fiber (PCF) [21]. The work in [22] reports the transportation of 400Gbit/s binary data over 120 m transmission range using 4 distinct orbital angular momentum (OAM) beams. In another work [23], 16-QAM signals are reported to carry 40Gbit/s data over 260 m of FSO link using 2-OAM beams with $\ell = +3\, and \ell = -3$. The transportation of 5Gbit/s-20GHz information over 500 m transmission range using Hermite Gaussian (HG) modes has been numerically simulated in [24]. The numerical simulations reporting the transportation of two Laguerre Gaussian (LG) beams with distinct azimuthal index and radial index to carry 200Gbit/s data over 1 m transmission range has been discussed in [25]. The work in [26] reports the simulative investigation of transportation of phase shift keying (PSK) encoded 40Gbit/s-80GHz information under clear conditions up to 50 km range using HG and LG beams. In [27], the performance of a 5Gbit/s-20GHz RoFSO link using distinct HG and LG beams has been compared for non return to zero (NRZ) and alternative mark inversion (AMI) schemes. The results exhibit reliable transmission of data up to 14 km range using AMI scheme. The work in [28] shows the transportation of 7.5Gbit/s-15GHz binary information up to 2.5 km range over two LG beams. The work in [29] exhibits the investigation of solid core photonic crystal fiber (SC-PCF) based MDM-RoFSO transmission system. The results exhibit a reliable transportation of 5Gbit/s-10GHz information up to 2.5 km range under dynamic weather conditions. The designing and numerical simulation of 100 Gbit/s FSO link incorporating hybrid MDM-optical code division multiple access (OCDMA) techniques up to 8 km transmission range under clear weather has been discussed in [30]. The performance comparison of pre-, booster, and inline amplifier configurations in a multi-input multi-output (MIMO) MDM based multimode fiber link over 100 km link range is discussed in [31]. The results show that inline amplifier configuration demonstrates the best results in terms of maximum link reach. The authors in [32] report a 100m-320 Gbit/s MDM based FSO link using doublet lens scheme. The performance investigation of $4 \times 4, 6 \times 6, and\ 9 \times 9$ MIMO-MDM based multimode fiber link using linear polarized (LP) modes is demonstrated in [33]. The work in [34] demonstrates the performance investigation of 10 Tbit/s hybrid WDM-MDM based multimode fiber link using LP modes for short-reach applications. In another work [35], demonstrates the modeling and simulative investigation of 2×2 MIMO enabled hybrid mode group division multiplexing (MGDM)-wavelength division multiplexing (WDM) with distributed antenna system for millimeter wave communication. The work in [36] reports the performance investigation of hybrid MDM-Dense WDM based passive optical network for Fiber-to-the-home services.

The main motivation of this work is as follows: (1) to design a large-capacity long-reach RoFSO transmission system by incorporating hybrid OFDM-MDM techniques (2) to analyze the proposed link performance under the influence of increasing divergence angle and dynamic atmospheric conditions (3) to report an improved performance investigation of the proposed system under adverse weather conditions by using an enhanced detection technique at the receiving unit and comparing the numerical results with existing system. The remainder of the paper is organized as- Section 2 covers system design and channel modeling. The results of the numerical investigation of the proposed link are presented in Section 3. The conclusion is given in Section 4.

2. System design

Fig. 1 exhibits the OFDM-MDM based hybrid RoFSO transmission system with enhanced detection which has been modeled using Optisystem™ simulation software v.15.

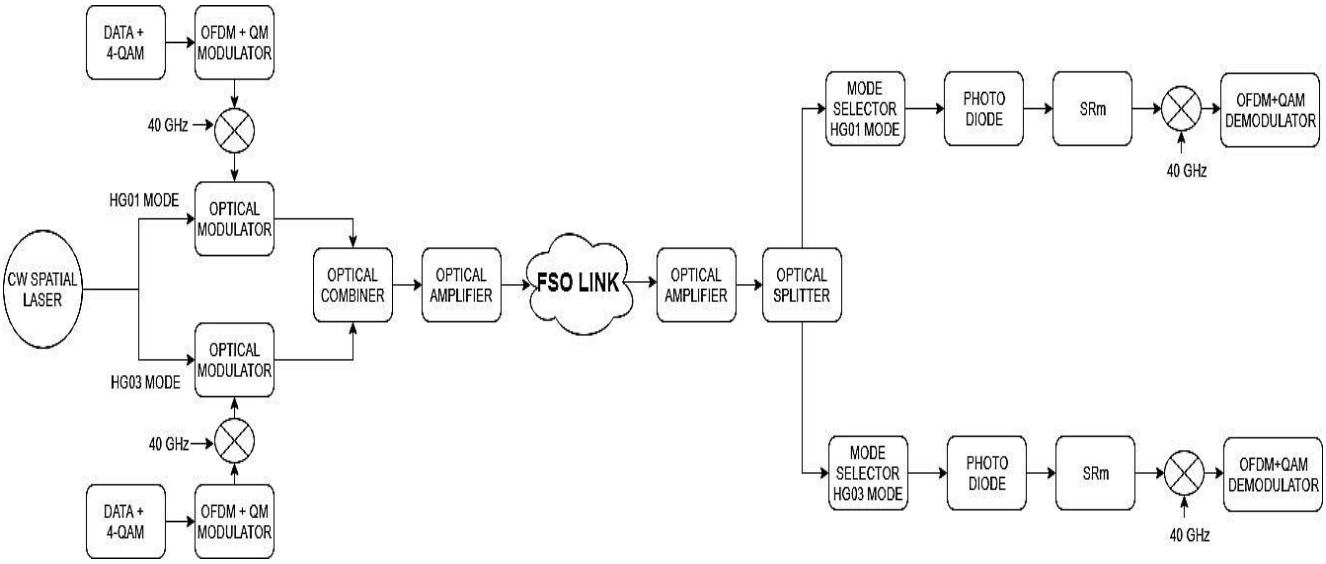

Fig. 1. Block diagram of the proposed RoFSO transmission system with enhanced detection

Two independent 20Gbit/s-40GHz binary information channels are transported simultaneously exploiting two distinct HG modes (HG01 and HG03) over free space medium under strong atmospheric turbulence. The HG modes are mathematically described as [37]:

$$\varphi_{m,n}(x,y) = H_m\left(\frac{\sqrt{2}x}{\omega_{0,x}}\right)\exp\left(-\frac{x^2}{\omega_{0x}^2}\right)\exp\left(j\frac{\pi x^2}{\lambda R_{ox}}\right)\times H_n\left(\frac{\sqrt{2}y}{w_{o,y}}\right)\exp\left(-\frac{y^2}{w_{oy}^2}\right)\exp\left(j\frac{\pi y^2}{\lambda R_{oy}}\right) \quad (1)$$

where R is the radius of curvature, m is the mode dependency on x-polarization axis, n is the mode dependency on y-polarization axis, w_o is the spot size at the waist of the beam, and H_m *and* H_n are Hermite polynomials. Fig. 2 exhibits distinct HG modes generated using a continuous wave (CW) spatial laser followed by a vortex lens.

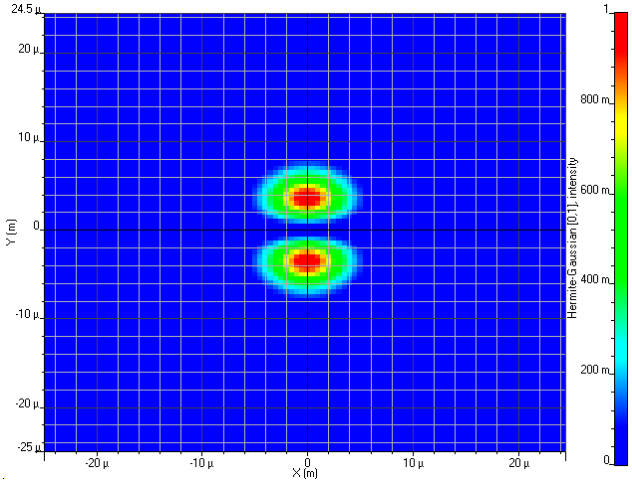

(a)

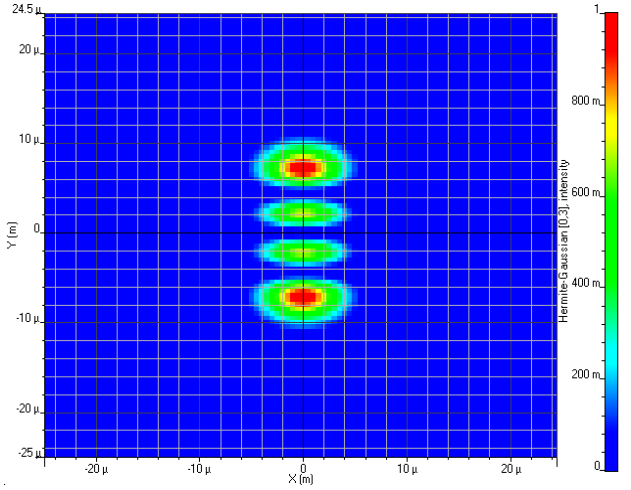

(b)

Fig. 2. Generated HG modes (a) HG01 mode (b) HG03 mode

20Gbit/s binary information signal is generated with a 4-QAM generator using 2-bits per symbol. This binary signal is then OFDM modulated over 1024 FFT points, 512 subcarriers and 32 prefix points. The OFDM signal is modulated over 40 GHz RF signal by a 7.5 GHz QAM modulator. The resulting 20Gbit/s-40GHz signal is transmitted using distinct HG mode over the free space channel. The link is mathematically described as [38]:

$$P_{Received} = P_{Transmitted}\left(\frac{d_R^2 Z}{(d_T + \theta Z)^2}\right)10^{-\alpha Z/10} \quad (2)$$

where d_R is the diameter of the receiving antenna, d_T is the diameter of the transmitting antenna, θ is the angle of beam divergence in $mrad$, Z is the link range, and α is the specific attenuation constant value determined by the weather condition. In this work, the diameter of the transmitting and the receiving antenna is taken as 10 cm, angle of beam divergence is taken as 0.25 $mrad$, and the specific attenuation constant value is taken as 0.155 dB/km for clear weather; 9 dB/km for thin fog; 12 dB/km for moderate fog; and 16 dB/km for heavy fog [39]. At the receiver unit, the received information signal is amplified by an optical amplifier with 20dB flat-gain and 4 dB noise figure. This signal is then directed towards an optical splitter followed by a mode selector for separation of distinct HG modes using non-interferometric modal decomposition. This signal is converted into an electrical signal using a spatial PIN photodiode. Further, the demodulation of this signal is done using a QAM demodulator and an OFDM demodulator followed by a QAM decoder for retrieving the information signal.

In this work, Beers-Lambert law is used to model atmospheric loss which can be described as [40]:

$$h_l = e^{-\sigma Z} \quad (3)$$

where σ is the specific attenuation constant value and Z is the link range. The atmospheric turbulence offered by different fog conditions can be reliably modeled by gamma-gamma (GG) distribution. The probability density function (pdf) for GG channel with h_a as optical irradiance is given as [41]:

$$f_{h_a}(h_a) = \frac{2(\alpha\beta)^{(\alpha+\beta)/2}}{\Gamma(\alpha)\Gamma(\beta)}h_a^{[(\alpha+\beta)/2]-1}K_{\alpha-\beta}\left(2\sqrt{\alpha\beta h_a}\right) \quad (4)$$

where Γ is the gamma function, α *and* β are the effective number of large scale and small scale eddies, , $K_{\alpha-\beta}$ is the modified Bessel function having order $(\alpha-\beta)$ which is simplified by using Meiger G function. The values of α *and* β for a spherical wave can be determined using:

$$\alpha = \left\{\exp\left[\frac{0.49\beta_o^2}{\left(1+0.18d^2+0.56\beta_o^{\frac{12}{5}}\right)^{\frac{7}{6}}}\right] - 1\right\}^{-1} \quad (5)$$

$$\beta = \left\{ \exp\left[\frac{0.51\beta_0^2 \left(1 + 0.69\beta_o^{\frac{12}{5}}\right)^{\frac{-5}{6}}}{\left(1 + 0.90d^2 + 0.62d^2\beta_o^{\frac{12}{5}}\right)^{\frac{5}{6}}} \right] - 1 \right\}^{-1} \quad (6)$$

where λ is the operating wavelength, $\beta^2 = 0.5C_n^2 k^{\frac{7}{6}} Z^{\frac{11}{6}}$ is the Roytov variance, k=$\frac{2\pi}{\lambda}$ is the optical wave number, C_n^2 is the index refraction structure parameter and its value is $10^{-9}m^{-2/3}$ under strong atmospheric turbulence. The specific attenuation constant value under different fog conditions can be reliably approximated using [42]:

$$\beta_{fog}(\lambda) = \frac{3.91}{V}\left(\frac{\lambda}{550}\right)^{-p} \quad (7)$$

where V is the range of visibility in km, λ is the wavelength in nm and p is the scattering distribution coefficient which can mathematically be calculated using Kim model as [43]:

$$p = \begin{cases} 1.6 & V > 50 \\ 1.3 & 6 < V < 50 \\ 0.16V + 0.34 & 1 < V < 6 \\ V - 0.5 & 0.5 < V < 1 \\ 0 & V < 0.5 \end{cases} \quad (8)$$

and Kruse model as [44]:

$$p = \begin{cases} 1.6 & V > 50 \\ 1.3 & 6 < V < 50 \\ 0.585V^{\frac{1}{3}} & V < 6 \end{cases} \quad (9)$$

At 1550 nm operating wavelength, the specific attenuation constant value is calculated as 9 dB/km for thin fog; 12 dB/km for moderate fog; and 16 dB/km for heavy fog. The geometric loss (A_{Geo}) with increasing transmission range is shown in Fig. 3 which can be reliably approximated using the following equation [45]:

$$A_{Geo} = 10log_{10}\left[\frac{4A_{RX}}{\pi(\theta Z)^2}\right]\text{dB} \quad (10)$$

where A_{RX} denotes the area of receiver surface, θ is the beam divergence angle in $mrad$, and Z is the FSO link range in km.

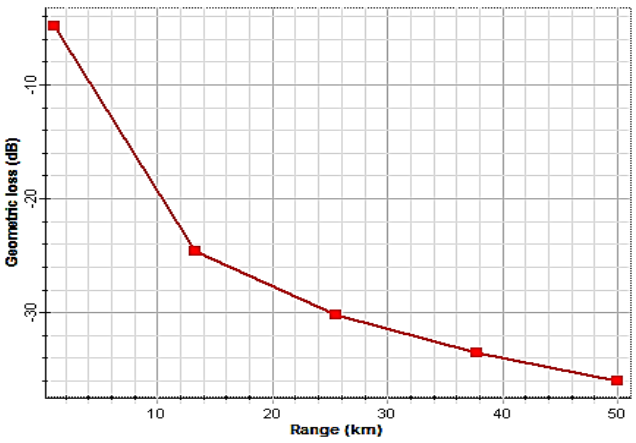

Fig. 3. Geometric Loss v/s FSO link range

3. Results and discussions

The numerical simulation results analyzing the performance of the proposed system under dynamic atmospheric conditions are reported in this section. Also, an enhanced performance analysis using SRm at the receiver terminal is reported in the later part.

3.1. Numerical investigation of the link performance under the impact of atmospheric turbulence

Fig. 4 (a) and (b) exhibit the performance of the proposed link under clear weather in terms of signal-to-noise ratio (SNR) and received power plots respectively. The results in Fig. 4 show that the SNR for channel 1 (HG01 mode) is reported as 39.63 dB, 27.12 dB, and 19.10 dB at a transmission range of 10 km, 30 km, and 50 km respectively whereas for channel 2 (HG 03 mode), SNR is reported as 37.84 dB. 25.83 dB, and 18.29 dB at a transmission range of 10 km, 30 km, and 50 km respectively. Similarly, the total power of the received signal for channel 1 is 0.76 dBm, -24.21 dBm, and -37.61 dBm and for channel 2 is -5.26 dBm, -29.87 dBm, and -44.06 dBm at a transmission range of 10 km, 30 km, and 50 km respectively. Fig. 5 and 6 exhibit RF spectrum and constellation diagram of the received signals respectively. Fig. 7 shows the decomposition of distinct HG modes at the receiving unit.

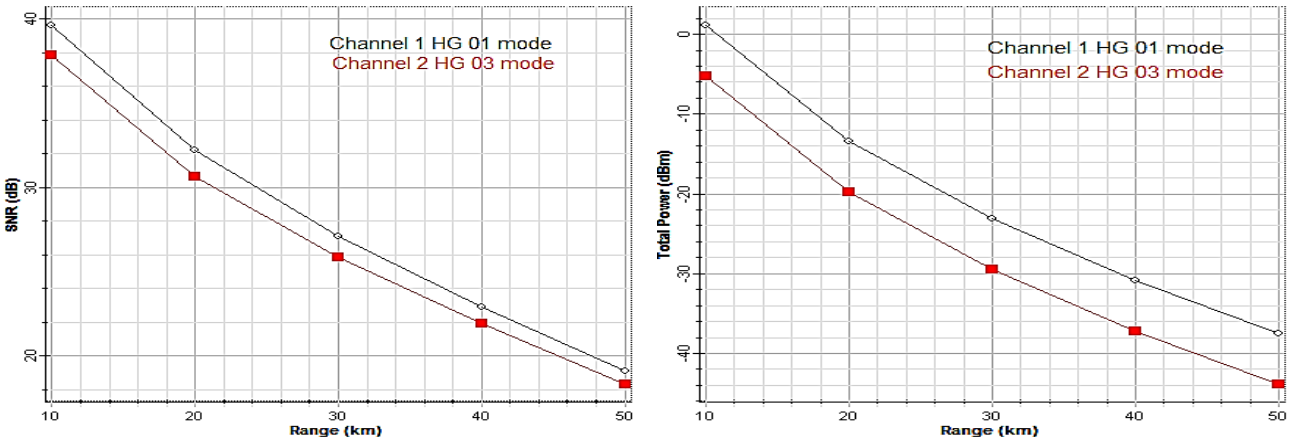

(a) (b)

Fig. 4. Evaluation of (a) SNR (b) Received power v/s link range under clear weather conditions

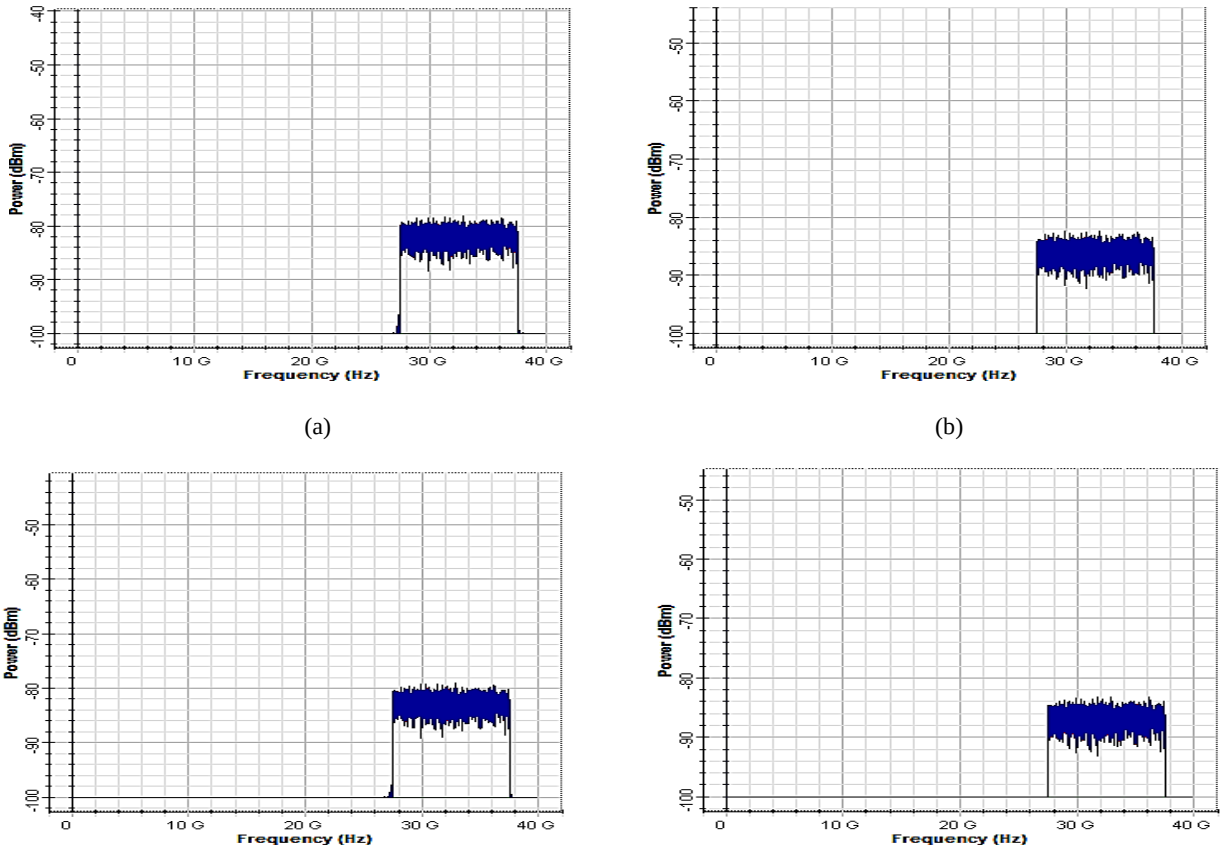

(a) (b)

(c) (d)

Fig. 5. RF spectrum (a) channel 1 (HG01 mode) at 30 km (b) channel 1 (HG01 mode) at 50 km (c) channel 2 (HG03 mode) at 30 km (d) channel 2 (HG03 mode) at 50 km

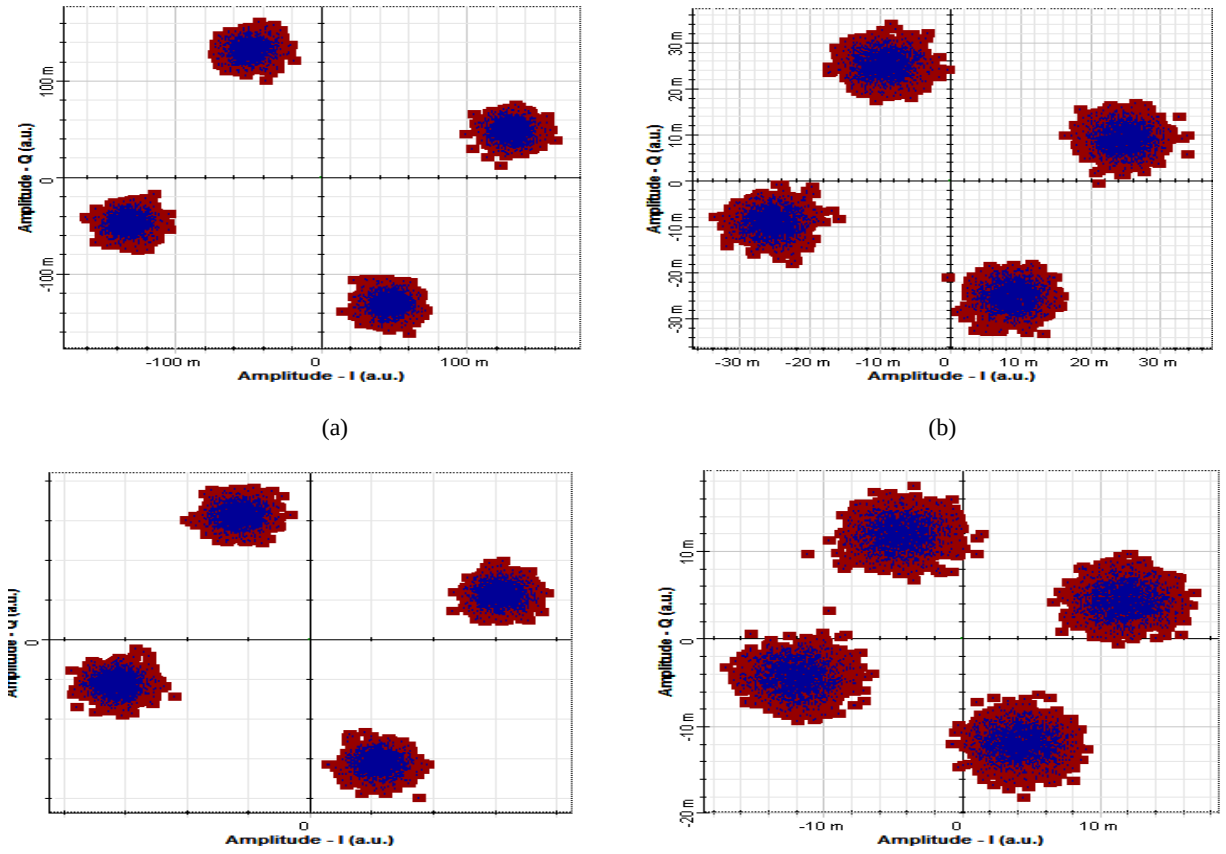

Fig. 6. Constellation diagrams (a) channel 1 (HG01 mode) at 30 km (b) channel 1 (HG01 mode) at 50 km (c) channel 2 (HG03 mode) at 30 km (d) channel 2 (HG03 mode) at 50 km

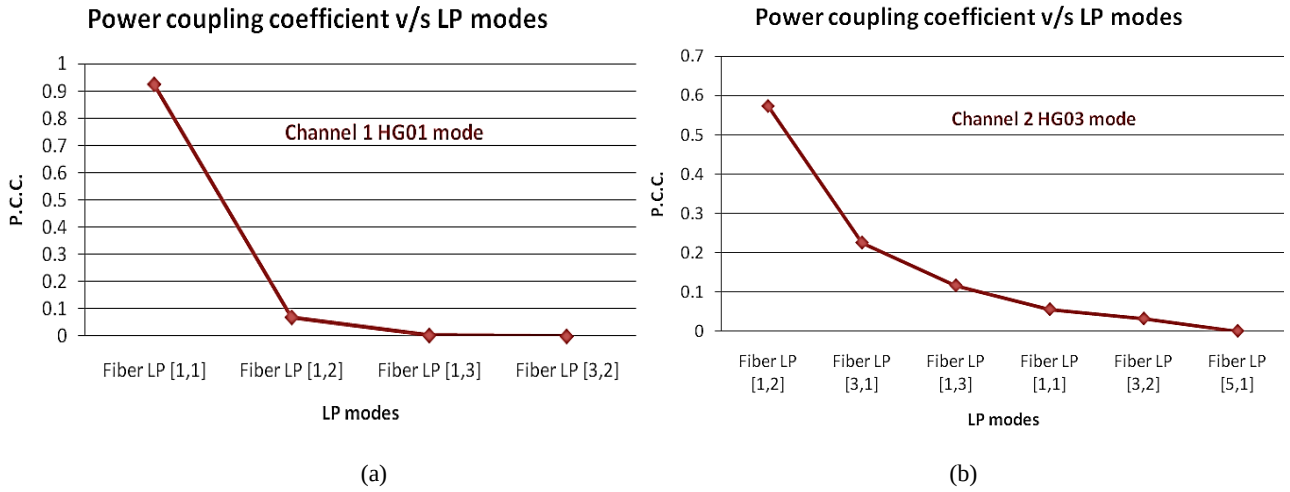

Fig. 7. Modal decomposition of distinct channels at the receiver terminal for (a) channel 1 (HG01 mode) (b) channel 2 (HG03 mode)

The RF spectrum of the received signals presented in Fig. 5 shows that on increasing the transmission range, the RF power reduces. Also, more RF power is collected by HG01 mode as compared to HG03 mode which shows that HG01 mode has more tolerance to multipath fading effects as compared to HG03 mode which is worst affected by it. The constellation diagrams of the received signals presented in Fig. 6 demonstrate that both the channels show precise constellation diagrams at a link distance of 30 km but as the link distance is increased to 50 km, the constellation diagrams are distorted. Also, constellation diagram for HG01 mode is clearer as compared to HG03 mode which shows higher distortion in HG03 mode with distance as compared to HG01 mode. Fig. 7 shows that

for channel 1 (HG01 mode) the power in predominantly coupled into LP11 mode followed by LP12, LP13, and LP32 mode whereas for channel 2 (HG03 mode), the most dominant mode is LP12 followed by LP31, LP13, LP11, LP32, and LP51. The results presented show that less coupling of modes occurs in channel 1 (HG01 mode) as compared to channel 2 (HG03 mode) which validates the results presented in performance analysis of the proposed link in Fig. 4. The effect of increasing angle of beam divergence on the performance of the proposed link is presented in Fig. 8, 9 and 10.

The results presented in Fig. 8 report that the SNR value decreases from [38.07, 36.31] dB to [23.92, 22.83] dB for channel 1 (HG01 mode) and channel 2 (HG03 mode) respectively as the angle of beam divergence increases from 0.25-1.50 $mrad$. Similarly, the received power reduces from [-1.92, -8.38] dBm to [-28.99, -35.45] dBm for channel 1 (HG01 mode) and channel 2 (HG03 mode) respectively as the angle of beam divergence increases from 0.25-1.50 $mrad$. Also, the RF spectrum and the constellation diagram of the received signals shown in Fig. 9 and 10 respectively demonstrate that as the angle of beam divergence increases, the RF power of the received signals reduces and the constellation diagram gets distorted.

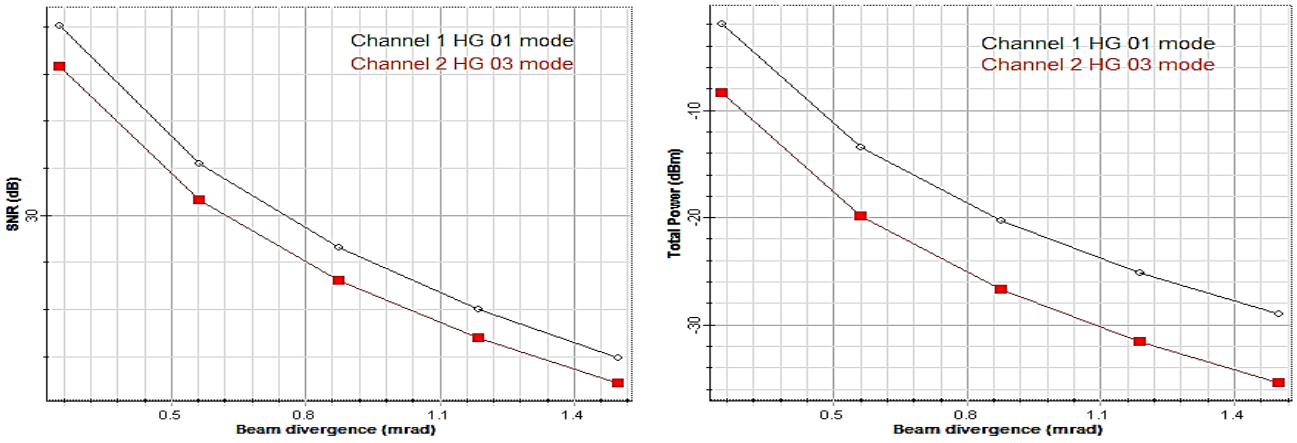

(a) (b)

Fig. 8. Measured (a) SNR (b) Received power under the impact of increasing beam divergence angle

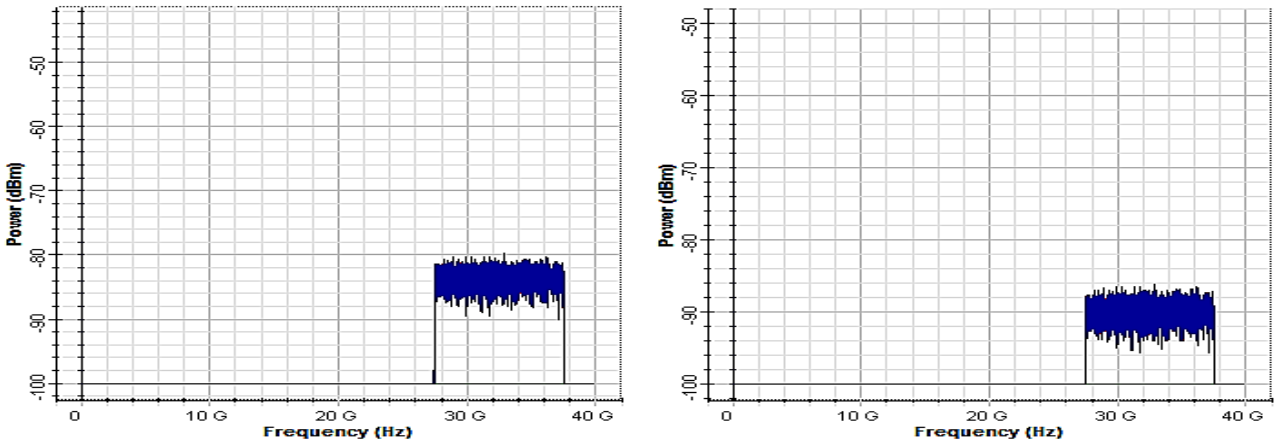

(a) (b)

Fig. 9. RF spectrum of the received signal for (a) channel 1 (HG01 mode) (b) channel 2 (HG03 mode) at 1.5 mrad divergence angle

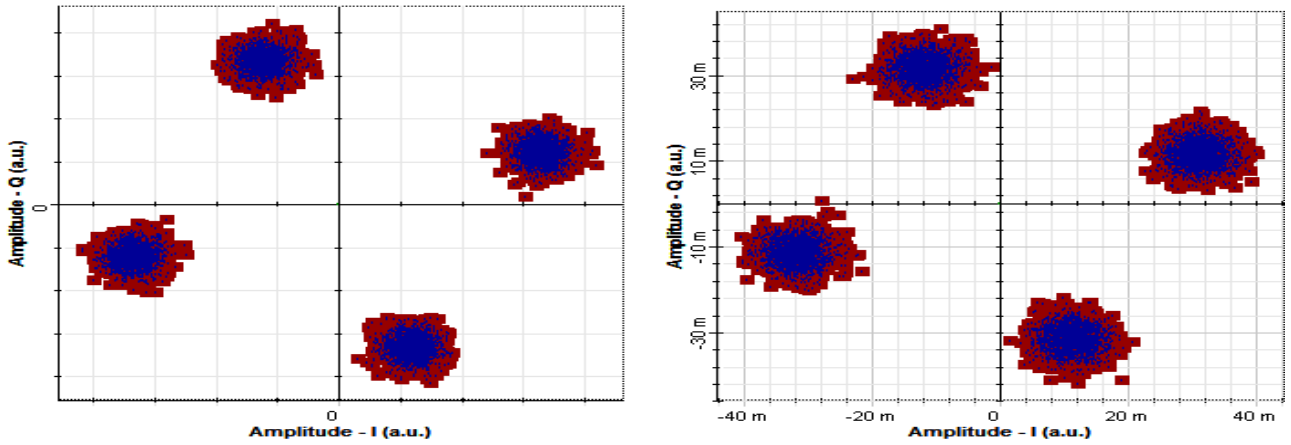

(a) (b)

Fig. 10. Constellation diagram of the received signal for (a) channel 1 (HG01 mode) (b) channel 2 (HG03 mode) at 1.5 mrad divergence angle

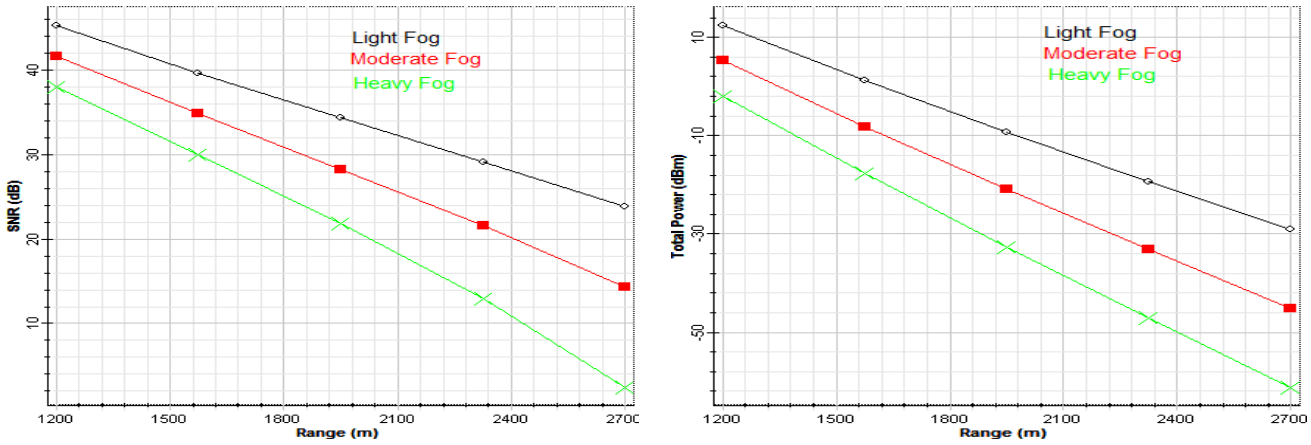

(a) (b)

Fig. 11. Measured (a) SNR (b) Received power v/s Link range under the impact of atmospheric turbulence

Further, we investigate the proposed link performance under the impact of adverse weather conditions. Fig. 11 reports that the SNR is computed as 45.34 dB, 34.35 dB, and 23.90 dB under light fog; 41.71 dB, 28.29 dB, and 14.27 dB under moderate fog; and 38.07 dB, 21.90 dB, and 2.36 dB under heavy fog conditions at a transmission range of 1200 m, 2000 m, and 2700 m respectively. Similarly, received power is computed as 12.47 dBm, -9.20 dBm, and -29.01 dBm under light fog; 5.27 dBm, -20.90 dBm, and -45.21 dBm under moderate fog; -1.92 dBm, -32.60 dBm, and -61.33 dBm under heavy fog conditions at a transmission range of 1200 m, 2000 m, and 2700 m respectively. The results of the simulative investigation of the proposed link exhibit that under clear weather, the maximum transmission range is 50 km whereas transmission range reduces to 2800 m, 2350 m, and 2000 m under light fog, moderate fog, and heavy fog respectively with acceptable performance levels (SNR$\sim 20dB$).

3.2. Enhanced performance analysis of the proposed link

In this section, we report the enhanced performance of the proposed link by using a Square root module (SRm) after the PIN photodiode at the receiver terminal. The temporal dispersion in FSO links posses limitation on the data transmission rates thus decreases the bandwidth of the channel. The scattering of the signal due to different atmospheric conditions results in temporal dispersion of the information signal transmitted due to multiple propagation paths thus leading to inter symbolic interference (ISI). The quadratic transfer function of the PIN photodiode used at the receiving unit transfers this linear distortion into a non-linear distortion and degrades the quality of the received signal. A SRm device has been proposed at the receiver terminal after the PIN photodiode which compensates for the non-linear response of the photodiode. SRm device can practically be achieved by deploying Schottky diodes [46]. Fig. 12 shows the ideal

(dashed-line) and non-ideal transfer characteristics of SRm. From Fig. 12, it can be seen that within useful current margin, the filtering error of practical SRm device is less than 10% with respect to the ideal conditions. The SRm device placed after PIN photodiode performs the inverse operation of square-law behavior as performed by PIN photodiode. The SRm device improves the system tolerance against temporal dispersion by linearizing the non-linear distortion. Further, the performance of the proposed link is enhanced by deploying a linear electrical equalizer for recovering the transmitted signal. The use of SRm device in the receiver has the following merits: (1); reduced number of required equalization levels for ADC (2) improved FSO link performance by linearization of optical impairments like optical noise, reflection etc.; (3) increase in temporal dispersion tolerance arising due to scattering; (4) easy and low cost application; (5) improvement in the FSO link power budget [46].

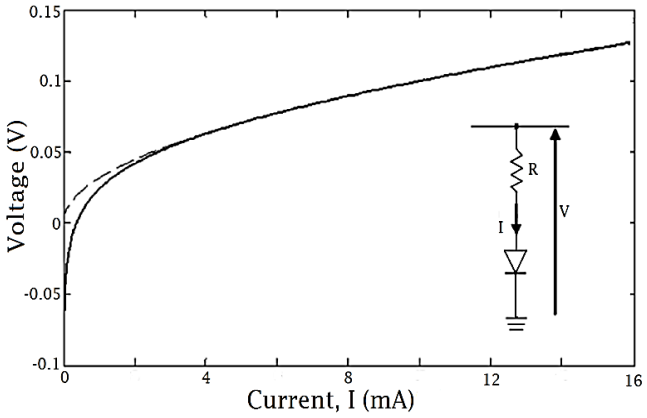

Fig. 12. Ideal (dashed line) and non-ideal transfer characteristics of the proposed SRm device [46]

Fig. 13 demonstrates the enhanced performance of the proposed link by deploying SRm at the receiving unit. Fig. 13 exhibits that SNR reduces from 38.07 dB to -67.79 dB in the link range of 1200 m to 4800 m without using SRm. Alternatively, SNR reduces from 85.64 dB to 10.16 dB in the link range of 1200 m to 4800 m with the use of SRm. Further, it can also be observed that total power of the received signal reduces from -1.92 dBm to -80.95dBm in the link range of 1200 m to 4800 m without using SRm whereas the total power reduces from 18.72 dBm to -43.74dBm in the link range of 1200 m to 4800 m with the use of SRm. The results presented show an effective improvement in SNR and received power in the proposed link by deploying SRm which will further lead to increasing the FSO transmission link range. The maximum link reach with acceptable performance (SNR~$20dB$) under heavy fog conditions using existing system is 2000 m which increases to 4400 m using the proposed enhanced detection technique. Thus, by deploying the proposed enhanced detection technique in FSO links, the effect of temporal dispersion due to adverse weather conditions like heavy fog can be mitigated and the link reach can be enhanced. Fig. 14 demonstrates the constellation diagrams of the received signals with and without SRm at the receiver terminal.

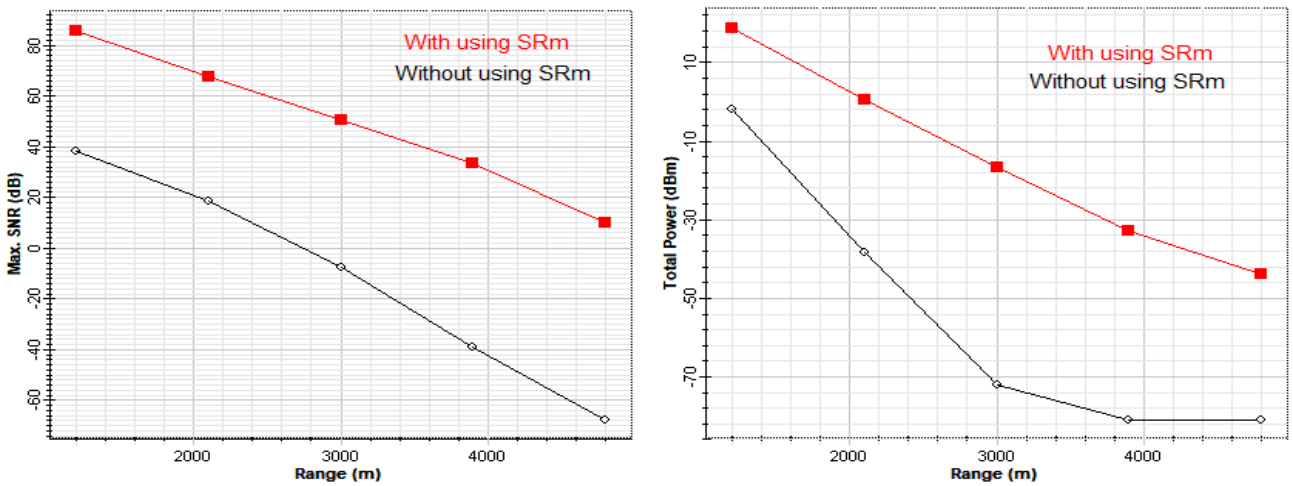

(a) (b)

Fig. 13. Measured (a) SNR (b) Received power v/s Link range with and without SRm at the receiver terminal

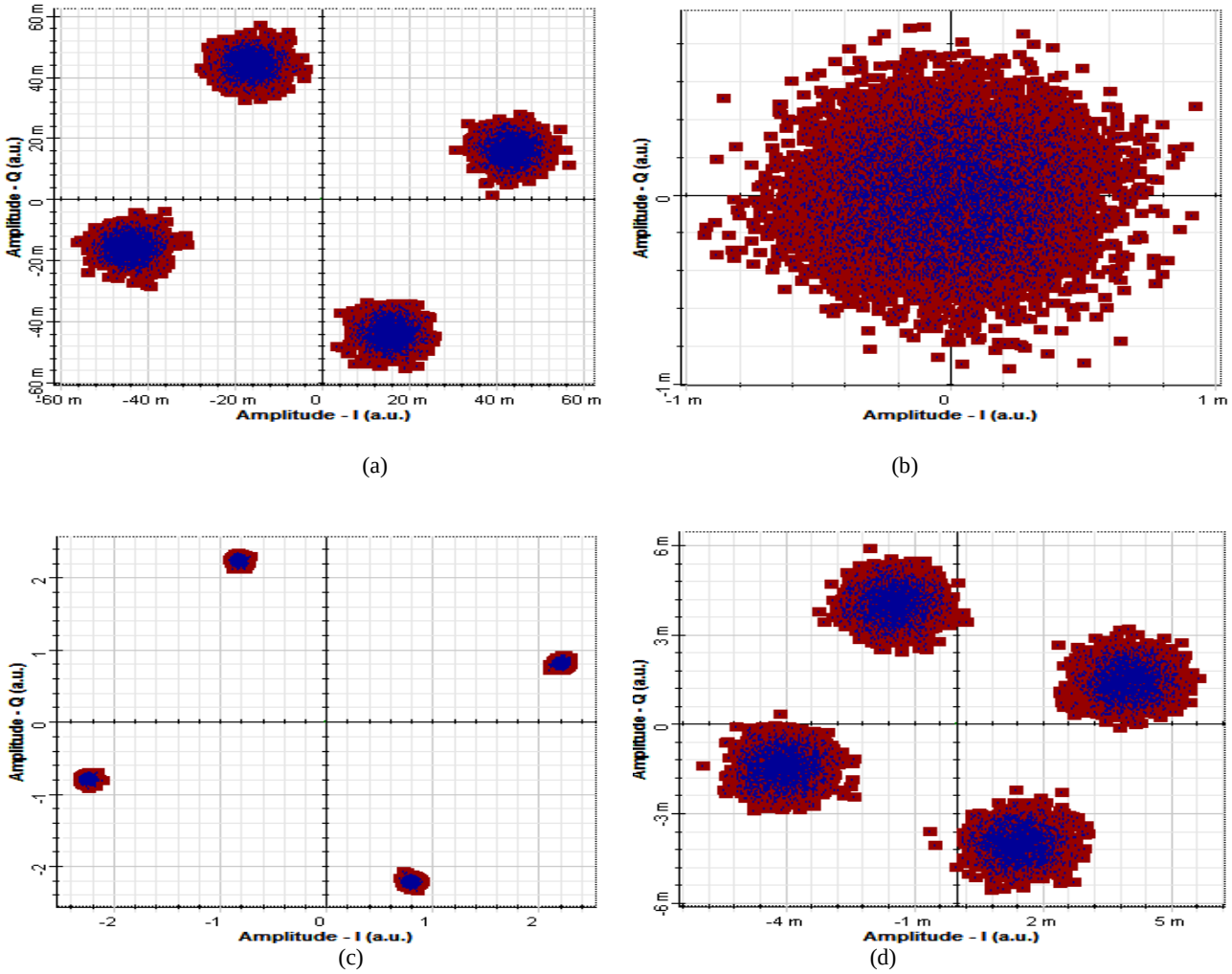

Fig. 14. Constellation diagram (a) without SRm at 2000 m (b) without SRm at 4400 m (c) with SRm at 2000 m (d) with SRm at 4400 m

4. Conclusion

In this work, 40Gbit/s-80GHz information is reliably transmitted over OFDM based RoFSO link by incorporating MDM of HG01 and HG03 modes under the impact of strong turbulence conditions and different weather conditions. The results of the simulative investigation of the proposed link conclude that the maximum achievable transmission range varies from 50 km to 2 km depending on the weather condition. Also, from the results presented it can be concluded that there is an effective improvement in the performance of the proposed link in terms of SNR and received power by using the proposed enhanced detection technique which will further help to enhance the transmission link distance of the system.

References

[1] M. A. Khalighi, M. Uysal, IEEE Communications Surveys & Tutorials **16** (4), 2231 (2014).
[2] A. Mahdy, J. S. Deogun, Proc. of IEEE Wireless Communications and Networking Conference **4**, 2399 (2004).
[3] G. Nykolak, P. F. Szajowski, G. Tourgee, H. Presby, Electronic Letters **35**(7), 578 (1999).
[4] S. A. Al-Gailani, A. B. Mohammad, R. Q. Shaddad, Proc. of IEEE 3rd International Conference on Photonics 121 (2012).
[5] A. Ramezani, M. R. Noroozi, M. Aghababaee, International Journal of Engineering and Advanced Technology **4**(1), 46 (2014).
[6] Jitendra Singh, Naresh Kumar, Optik - International Journal of Light and Electron Optics **124**(20), 4651 (2013).
[7] S. Attri, C. Narula, S. Kumar, Proc. of International Conference on Intelligent Communication, Control, Devices 167 (2016).
[8] V. Sharma, G. Kaur, Optik **124**, 6111 (2013).
[9] J. M. Tang, P. M. Lane, K. A. Shore, J. Lightw. Technol.**24**, 429 (2006).
[10] Q. Yang, W. Shieh, Y. MaIEEE Photon. Technol. Lett. **20**, 1305 (2008).

[11] K. Forozesh, S. L. Jansen, S. Randel, I. Morita, H. Tanaka, presented at the IEEE/LEOS Summer Topical Meetings, 2008.
[12] D. Dardari, IEEE Trans. Circuits Syst. I: Fundamental Theory Applicat. **53**, 1741 (2006).
[13] W. Shieh, IEEE Photon. Technol. Lett. **19**, 134 (2007).
[14] S. L. Jansen, I. Morita, H. Tanaka, Proc. ECOC (2007).
[15] S. Randel, R. Ryf, A. Sierra, P. J. Winzer, A. H. Gnauck, C. A. Bolle, R. J. Essiambre et al., Proc. of Optical Fiber Communication Conference and Exposition (OFC/NFOEC), 1 (IEEE, Los Angeles, 2011).
[16] A. Amphawan, O. Dominic, Proc. of Photonics (ICP), International Conference (IEEE, Langkawi, 2010).
[17] A. Amphawan, V. Mishrab, K. Nisaran, B. Nedniyomc J. Mod. Optic. **59**, 1745 (2012).
[18] A. Amphawan, Opt. Express **19**, 23085 (2011).
[19] A. Amphawan, J. Mod. Optic. **59**, 460 (2012).
[20] Y. Jung, R. Chen, R. Ismaeel, G. Brambilla, S. U. Alam, I. P. Giles, D. J. Richardson, Opt. Express **21**, 24326 (2013).
[21] A. Amphawan, N. Benjaporn, M. A. S. Nashwan, J. Mod. Optic **49**, 1 (2014).
[22] Y. Ren, Z. Wang, P. Liao, L. Li, G. Xie, H. Huang, et al., Opt. Lett. **41**, 622 (2016).
[23] Y. Zhao, J. Liu, J. Du, S. Li, Y. Luo, A. Wang et al., Optical Fiber Communication Conference 13 (2016).
[24] A. Amphawan et al., International Conference on Optical and Photonic Engineering (icOPEN2015), International Society for Optics and Photonics, pp. 95242H (2015).
[25] G. Xie et al., Opt. Lett. **41**, 3447 (2016).
[26] S. Chaudhary, B. Lin, X. Tang, X Wei, Z. Zhou, C. Lin, M. Zhang, H. Zhang, Optical and Quantum Electronics **50**, 321 (2018).
[27] SushankChaudhary, Angela Amphawan, International Journal of Electronics Letters **7**(3), 304 (2019).
[28] Sushank Chaudhary, Angela Amphawan, Laser Physics **27**(7), 075106 (2018).
[29] Sushank Chaudhary, Angela Amphawan, Photonic Network Communication **36**(2), 263 (2018).
[30] Himali Sarangal, Amarpal Singh, Jyoteesh Malhotra, Sushank Chaudhary, Opt. Quant. Electon. **49**, 184 (2017).
[31] Rajan Gupta, Rajinder Singh Kaler, Optical Engineering **55**(5), 056102 (2016).
[32] Chung-Yi Li et al., Laser Physics Letters **13**, 075201 (2016).
[33] Rajan Gupta,Rajinder Singh Kaler, Optoelectron. Adv. Mat. **11**(11-12), 643 (2017).
[34] Rajan Gupta, Rajinder Singh Kaler, Optoelectron. Adv. Mat. **12**(7-8), 441 (2018).
[35] A. Raja, S.Gahfoor, M. F. U. Butt, Photonic Network Communication **35**, 265 (2018).
[36] Youseg Fazea, Optik **183**, 994 (2019).
[37] A. Ghatak, K. Thyagarajan, Cambridge University Press, Cambridge (1998).
[38] D. R. Kolev, K. Wakamori, M. Matsumoto, J. Lightwave Technol. **30**, 3727 (2012).
[39] H. Sarangal, A. Singh, J. Malhotra, S. Chaudhary, Opt. Quant. Electron.**49**, 184 (2017).
[40] L. Pan, C. Ding, H. Wang, Opt. Express **22**, 11670 (2014).
[41] A. Amphawan, W. A. Alabdalleh, Opt. Techn. Let. **54**, 1362 (2012).
[42] L. C. Andrews, R. L. Phillips, "Laser Beam Propagation Through Random Media" (2nd edition, SPIE Press Book, Bellingham WA,2005).
[43] I. Kim, B. Mcarthur, E. Korevaar, Proc. of SPIE Optical Wireless Communication**6303**, 26 (2006).
[44] P. W. Kruse, L. D. McGlauchlin, R. B. McQuistan, "Elements of infrared technology: Generation, transmission, and detection", Wiley, 1962.
[45] Recommendation ITU-R, P.1814, May 2—7.
[46] J. Prat, A. Napoli, J. M. Gene, M. Omella, P. Poggiolini, V. Curri, Proceedings of the ECOC 2005, Glasgow, UK, 106 (2005).

*Corresponding author: mehtab91singh@gmail.com